Ocean & Sea Ice SAF

The EUMETSAT OSI SAF AMSR-2 Sea Ice Concentration Algorithm

Algorithm Theoretical Basis Document

Product OSI-408

Version 1.0

February 2015

Tian Tian, Rasmus Tonboe, and John Lavelle

The EUMETSAT
Network of
Satellite Application
Facilities

OSI SAF
Ocean and Sea Ice

Documentation Change Record

Document version	Software version	Date	Change	Description
v 1.0	v 1.0	15/12/15		First version.
v 1.1		27/01/16	minor	After review.

The software version number gives the corresponding version of the OSI SAF High Latitude software chain which was used to produce the reprocessing data set.

CONTENTS

1. Introduction

1.1 OSI SAF overview

The Ocean and Sea Ice Satellite Application Facility, OSI SAF, is a EUMETSAT project that started in 1997. The OSI SAF is a part of the EUMETSAT distributed ground segment for production of operational near real time value added satellite products. The OSI SAF delivers a range of air-sea interface products, namely: sea ice characteristics, SST, radiative fluxes and wind over open water. The sea ice products are sea ice concentration, the sea ice emissivity and temperature, sea ice edge, sea ice type and sea ice drift.

The OSI SAF project is managed by CMS, Meteo-France. The sea ice products are produced at the OSI SAF High Latitude processing facility under the responsibility of the Norwegian Meteorological Institute, operated jointly by the Norwegian and Danish Meteorological Institutes.

1.2 Sea ice concentration algorithm

Since the start of the operational production of sea ice products in 2002 the growing user group has brought more focus on expanding the available data set in particular achieving higher spatial resolution. The AMSR-2 instrument has four times better resolution at comparable electromagnetic frequencies than the SSMIS which is currently used for sea ice concentration processing. The spatial resolution of the AMSR-2 89GHz channels is about 5 km.

1.3 Ownership and copyright of data

The OSI SAF sea ice concentration data has been produced under responsibility of Norwegian Meteorological Institute and Danish Meteorological Institutes. The ownership and copyrights of the data set belongs to EUMETSAT. The data set is distributed free of charge, but EUMETSAT must be acknowledged when using the data. EUMETSAT's copyright credit must be shown by displaying the words "copyright (year) EUMETSAT" on each of the products used. The user registration ensures that all users are informed about potential updates or processing anomalies and the feedback from users is important argumentation for the project team when defining new development activities. We urge anyone to use the data and provide feedback to the project team.

1.4 Glossary

ADEOS	Advanced Earth Observing Satellite
AMSR	Advanced Microwave Scanning Radiome
ATBD	Algorithm Theoretical Basis Doccument
CMS	Centre de Météorologie Spatiale
CDOP	Continuous Development and Operations Phase (OSI SAF project)
DMI	Danish Meteorological Institute
ECMWF	European Centre for Medium range Weather Forecast
ESA SICCI	European Space Agency Sea Ice Climate Change Initiative
EUMETSAT	European Organization for the Exploitation of Meteorological Satellites
FOV	Field of view
FWHM	Full width at half maximum
met.no	Norwegian Meteorological Institute
NASA	National Aeronautics and Space Administration
NT	NASA Team
NSIDC	National Snow and Ice Data Center
NWP	Numerical Weather Prediction
OSI SAF	Ocean and Sea Ice Satellite Application Facility

PM   Passive microwave
RTM   Radiative Transfer Model
SAR   Synthetic Aperture Radar
SICCI   Sea ice climate change initiative
SSM/I   Special Sensor Microwave/Imager
SMMR   Scanning Multi-channel Microwave Radiometer
SST   Sea surface temperature
TUD   Technical University of Denmark

1.5   Reference Documents

[RD.1] ATBD for OSI SAF Aqua AMSR-E ice concentration product (OSI-408), version 0.1. Available at http://osisaf.met.no/docs.

[RD.2] OSI SAF Global Sea Ice Concentration Reprocessing Product User Manual (OSI-409), version 1.3. Available at http://osisaf.met.no/docs.

[RD.3] ATBD for OSI SAF Global Reprocessed Sea Ice Concentration Product (OSI-409, OSI-409a, OSI-430), version 1.1. Available at http://osisaf.met.no/docs.
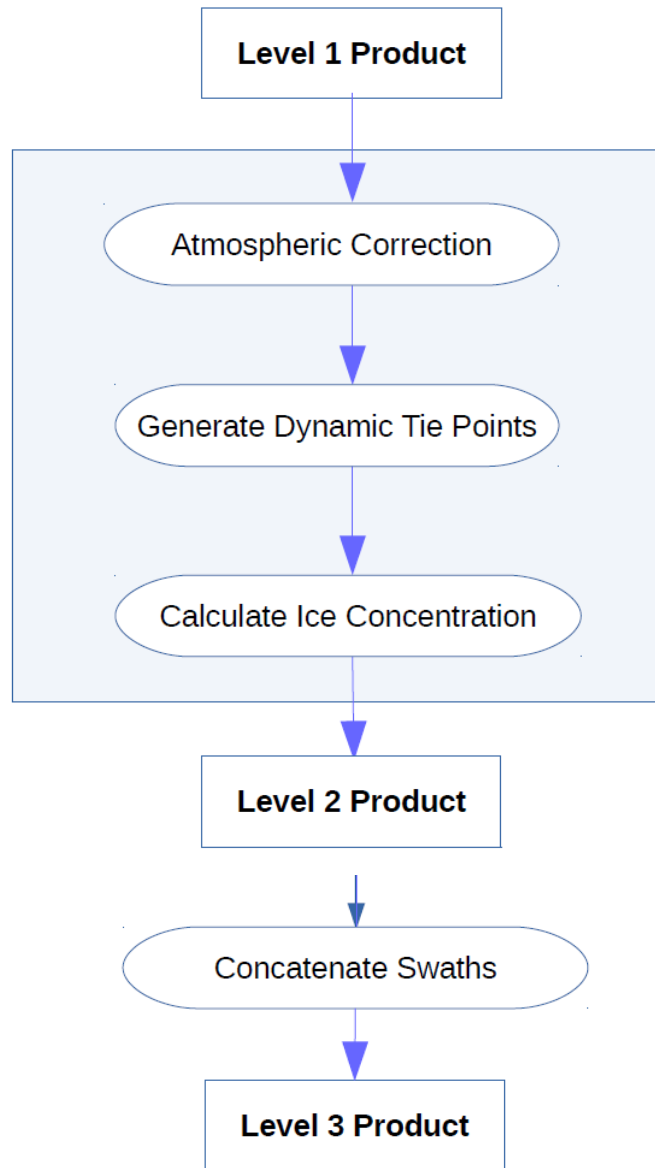
2.   Process Overview

Figure 1. Processing flow chart for the level 2 and 3 production.

The procedures for processing the daily level 2 and level 3 sea ice concentration products are schematically presented in Figure 1. In the first step, the Radiative Transfer Model (RTM) is applied for the atmospheric correction as described in Section 4.1. In the second step, the dynamic tie points are generated, as described in Section 4.2. In the third step, the ice concentration algorithm is applied, as described in Section 4.3. Finally, for the level 3 product, the swaths from each are concatenated, as described in Section 5.

3.   Input data

This chapter describes the AMSR-2 satellite data and the OSI SAF sea ice concentration algorithm which is applied to it. This algorithm may be applied to many types of microwave radiometer data, such as SSM/I, SMMR, and AMSR. Prior to calculating the sea ice concentration, the algorithm used NWP data for correction of the brightness temperatures. The NWP parameter fields are briefly described. It is important not to introduce potential biases from the NWP model. Therefore, we are using a procedure which is called "dynamical tie-points". The procedure is also described in section 4.2.

3.1   The AMSR-2 satellite data

The AMSR-2 instrument was launched in May 2012. It is a successor of AMSR on the Advanced Earth Observing Satellite-II (ADEOS-II) and AMSR for EOS (AMSR-E) on NASA's Aqua satellite. The AMSR-2 is a conically scanning Passive microwave (PM) radiometer system, with a constant incidence angle of 55° and a swath width of 1450 km. The frequency bands range from 6.925 GHz to 89.0 GHz with both horizontal and vertical polarizations. The channel characteristics are summarized in Table 1 (see Table 2 in Imaoka et al., 2010).

Table 1. AMSR-2 characteristics and performance

Center freq. (GHz)	Band width (MHz)	Beam width (3dB, deg)	Footprint size [km x km]	Sampling Interval (km)
6.925/7.3	350	1.8	35×62	10
10.65	100	1.2	24×42	10
18.7	200	0.65	14×22	10
23.8	400	0.75	15×26	10
36.5	1000	0.35	7×12	10
89.0	3000	0.15	3×5	5

Compared to AMSR-E, AMSR-2 provides several enhancements, including a larger main, 2.0 m diameter, offset parabolic reflector, additional channels in C-band receiver, and improved calibration system (Imaoka et al., 2010). Details about AMSR-E are available in [RD.1].

The sea ice concentration algorithm uses the input from brightness temperature swath data at three low frequency channels (19V, 37H and 37V) and two high frequency channels (89H and 89V).

3.2   NWP data for the RTM atmospheric correction

The atmospheric water content and wind roughening of the open sea surface can sometimes be problematic for sea ice concentration retrievals. The brightness temperatures (T_b) are corrected explicitly for wind roughening over open water and water vapor in the atmosphere prior to the calculation of ice concentration. The correction is using RTM and NWP data. Over areas with both ice and water the influence of open water roughness on the T_b's and the ice emissivity is scaled linearly with the ice concentration. The emissivity of ice is determined from standard tie-point emissivities. The correction procedure is described in detail in Andersen et al. (2006B). The NWP model grid points are co-located with the satellite swath data in time and space and a correction to the T_b 's is applied.

The following prognostic variables are taken from the ECMWF operational forecast model output: wind speed (W), 2m air temperature (Ts), total column water vapor (V), total column cloud liquid water (L).

Parameters such as Ts, W and V are well represented by the NWP models (at least in the short-term forecasts). However, the representation of cloud liquid water column in the NWP data is not suitable to use for T_b correction (see Andersen et al., 2006B). The T_b's are therefore not corrected for the influence of cloud liquid water following the procedure in Andersen et al. (2006B) and in Ivanova et al. (2015) where it is set to zero in the RTM. The RTM is described in Wentz (1997) and has been adopted by Wentz and Meissner (2000) for the AMSR processing. Based on these two references, the model is briefly described in the next section, section 4.1.

4.   Level 2 processing

In Level 2 processing, atmospheric correction is first applied to the AMSR-2 Level 1 global swath brightness temperatures (T_b) using RTM and NWP data. Secondly, the daily tie-points as reference values in the ice concentration algorithms are determined. With the inputs from the above two steps (Figure 1), the ice concentration is calculated using the OSISAF hybrid algorithm and the TUD hybrid algorithm, respectively. This chapter describes algorithms used in level 2 processing.

4.1   Tb correction for water vapor and open water surface roughness variability

Using the model function presented in this section, the T_b's are corrected for the influence of water vapor in the atmosphere and open water surface roughness caused by wind shear. The model function is a semi-empirical radiative transfer ocean model describing the T_b as a function of sea surface temperature, surface wind friction velocity, total atmospheric water vapor, total cloud liquid water and surface air temperature. The model function was used for SSMI processing and described in Wentz (1997), and it has been adopted by Wentz and Meissner (2000) for AMSR processing, with consideration of differences in frequencies, polarization and incidence angle from previous satellite radiometers.

The correction procedure is described in Andersen et al. (2006B). At intermediate ice concentrations the surface emission term is a linear combination of ice emissivity derived from tie-point signatures and the open water emissivity derived from the model.

The model function is using the simplified radiative transfer function for isotropic conditions (which is adequate for many applications including this one) together with regressions describing the sensitivity to atmospheric and surface parameters. The radiative transfer equation for the top of the atmosphere brightness temperature, F:

$$F(W,V,L)=T_{BU}+\tau[E \cdot T_S+(1-E)(\Omega \cdot T_{BD}+\tau \cdot T_C)], \tag{1}$$

where V (mm) is the vertically integrated water vapor, W (m/s) is the wind speed (at 10m) and L (mm) is the vertically integrated cloud liquid water (here $L=0$). T_{BU} and T_{BD} are the upwelling and down-welling atmospheric brightness temperatures and τ is the atmospheric transmittance. E is the sea surface emissivity and T_S is the sea surface temperature. T_C is the cosmic background radiation temperature equaling 2.7K. All temperatures are in kelvins. The Ω term is the reflection reduction factor due to wind induced sea surface roughness.

The upwelling and down-welling brightness temperatures are expressed in terms of effective air temperatures T_U and T_D, defined by

$$T_U = T_{BU} / (1-\tau) \tag{2a}$$

$$T_D = T_{BD} / (1-\tau). \tag{2b}$$

T_U is a few degrees colder than T_D. In Wentz (1997), T_U and T_D were found highly correlated with V and T_S at the radiosonde site. The following least squares regressions are given as (see Eq. 26-27 in Wentz and Meissner, 2000):

$$T_D = b_0 + b_1 V + b_2 V^2 + b_3 V^3 + b_4 V^4 + b_5 \varsigma (T_S - T_V) \tag{3a}$$

$$T_U = T_D + b_6 + b_7 V, \tag{3b}$$

where

$$T_V = 273.16 + 0.8337 V - 3.029 \cdot 10^{-5} V^{3.33} \qquad V \le 48 \tag{4a}$$

$$T_V = 301.16 \qquad V > 48 \tag{4b}$$

and

$$\varsigma(T_S - T_V) = 1.05(T_S - T_V)[1 - (T_S - T_V)^2 / 1200] \qquad |T_S - T_V| \leq 20\ K \qquad (4c)$$

$$\varsigma(T_S - T_V) = sign(T_S - T_V) \cdot 14K \qquad |T_S - T_V| > 20\ K \qquad (4d)$$

The regression coefficients b in Eq. 3 are given in Table 2. Equations 4a and 4b are found by regressing the T_S climatology at the radiosonde site to V. Thus T_V represents sea surface temperature for given water vapor in the atmosphere. Wentz and Meissner (2000) include a function of the difference between the sea surface temperature T_S and T_V. The term $\varsigma(T_S - T_V)$ accounts for the fact that the effective air temperature is typically higher (or lower) for the case of unusually warm (or cold) water. Here scattering by cloud liquid water is neglected.

Table 2. Model coefficients and constants for the Atmosphere

Freq.	19GHz	37GHz	89GHz
b_0 (K)	240.24	239.45	242.58
b_1 (K mm^{-1})	298.88E-2	254.41E-2	302.33E-2
b_2 (K mm^{-2})	-725.93E-4	-512.84E-4	-749.76E-4
b_3 (K mm^{-3})	814.50E-6	452.02E-6	880.66E-6
b_4 (K mm^{-4})	-36.07E-7	-14.36E-7	-40.88E-7
b_5	0.61	0.58	0.62
b_6 (K)	-0.16	-0.57	-0.57
b_7 (K mm^{-1})	-1.69E-2	-2.38E-2	-8.07E-2
a_{O1}	12.15E-3	40.06E-3	53.35E-3
a_{O2} (K)	-0.61E-4	-2.00E-4	-1.18E-4
a_{V1} (mm^{-1})	1.73E-3	1.88E-3	8.78E-3
a_{V2} (mm^{-1})	-0.05E-5	0.09E-5	0.80E-5
a_{L1}	0.0556	0.2027	0.9693
a_{L2}	0.0288	0.0261	0.0146

The total transmittance through the atmosphere along the line of sight, τ is given by

$$\tau = exp\,[-sec\theta\,(A_O + A_V + A_L)] \qquad (5)$$

where θ is the incidence angle, A_O, A_V and A_L denote the vertically integrated adsorption components to oxygen, water vapor and liquid water, respectively. The approximations for A_O, A_V and A_L are given as (see Eq. 28-33 in Wentz and Meissner, 2000):

$$A_O = a_{O1} + a_{O2}\,(T_D - 270) \qquad (6a)$$

$$A_V = a_{V1}V + a_{V2}\,V^2 \qquad (6b)$$

$$A_L = a_{L1}\,[1 - a_{L2}\,(T_L - 283)]\,L, \qquad (6c)$$

where L is in millimeters. T_L is approximated by $(T_S + 273)/2$, which is the mean temperature of the cloud. The a_O, a_V and a_L coefficients are given in Table 2 for all AMSR-2 channels used for calculating sea ice concentration.

The dielectric constant of sea water is a key component of the sea surface model. The parameter is a complex number that depends on frequency v, sea surface temperature T_S and water salinity s. The dielectric constant is given as (see Eq. 35 in Wentz and Meissner, 2000)

$$\varepsilon = \varepsilon_R + \frac{\varepsilon_S - \varepsilon_R}{1 + [j\lambda_R/\lambda]^{1-\eta}} - \frac{2j\sigma\lambda}{C} \,, \tag{7}$$

where $j = \sqrt{-1}$, $\lambda = c/(1E9v)$ in cm is the radiation wavelength and v is frequency. ε_R is the dielectric constant at infinite frequency, ε_S is the static dielectric constant, and λ_R (cm) is the relaxation wavelength. The spread factor η is an empirical parameter. The last term accounts for the conductivity of salt water, where σ (sec^{-1}) is the ionic conductivity and c is the speed of light ($3.0 \cdot 10^8$ m/s). It is generally assumed that η and ε_R are independent of temperature. The least squares fit yields $\eta = 0.012$ and $\varepsilon_R = 4.44$ (Wentz and Meissner, 2000).

Given the salinity s = 35 (‰), the conductivity of sea water is given by

$$\sigma = 3.39 \cdot 10^9 C^{0.892} \, exp(-\Delta_t \zeta) \tag{8}$$

$$C = 0.5536 \, s \tag{9a}$$

$$\Delta_t = 25 - t_S \tag{9b}$$

$$\zeta = 2.03 \cdot 10^{-2} + 1.27 \cdot 10^{-4} \Delta_t + 2.46 \cdot 10^{-6} \Delta_t^2 - C (3.34 \cdot 10^{-5} - 4.6 \cdot 10^{-7} \Delta_t + 4.6 \cdot 10^{-8} \Delta_t^2) \tag{9c}$$

where C is chlorinity in ‰ and $t_S = T_S - 273.15$ in Celsius units.

The effect of salinity on ε_S and λ_R are modelled as (see Eq. 43-44 in Wentz and Meissner, 2000):

$$\lambda_R = 3.30 \, exp(-0.0346 \, t_S + 0.00017 \, t_S^2) - 6.54 \cdot 10^{-3} (1 - 3.06 \cdot 10^{-2} \, t_S + 2.0 \cdot 10^{-4} \, t_S^2)s \tag{10}$$

$$\varepsilon_S = 87.9 \, exp(-0.004585 \, t_S) \, exp(-3.45E\text{-}3s + 4.69 \cdot 10^{-6}s^2 + 1.36 \cdot 10^{-5} \, s \cdot t_S) \tag{11}$$

Once the dielectric constant ε is known, the *v-pol* (vertical-polarisation) and *h-pol* (horizontal-polarisation) reflectivity coefficients ρ_V and ρ_h for a specular (i.e. perfectly flat) sea surface are calculated from the Fresnel equations:

$$\rho_v = \frac{\varepsilon \cos\theta - \sqrt{\varepsilon - \sin^2\theta}}{\varepsilon \cos\theta + \sqrt{\varepsilon - \sin^2\theta}} \tag{12a}$$

$$\rho_h = \frac{\cos\theta - \sqrt{\varepsilon - \sin^2\theta}}{\cos\theta + \sqrt{\varepsilon - \sin^2\theta}}, \tag{12b}$$

where θ is the incidence angle. The specular reflectivity R_0 is then given as (see Eq. 46 in Wentz and Meissner, 2000):

$$R_{0v} = |\rho_v|^2 + \Delta R_{0v} \tag{13a}$$

$$R_{0h} = |\rho_h|^2 \tag{13b}$$

$$\Delta R_{0v} = 4.887 \cdot 10^{-8} - 6.108 \cdot 10^{-8}(T_S - 273)^3 \tag{13c}$$

Wentz and Meissner (2000) proposed to add a correction term, as defined in eq. 13c, to the v-pol reflectivity. The correction can lead to changes in the brightness temperature range from about +0.14 K in cold water to about -0.36 K in warm water.

The microwave emission from the ocean depends on surface roughness. A calm sea surface is characterized by a highly polarized emission. When the surface becomes rough, the emission increases and becomes less polarized, except at $\theta > 55°$ for which the vertically polarized emission decreases.

The rough sea surface reflectivity R is given as:

$$R = (1 - E_W) R_{geo} \tag{14}$$

Where the reflectivity R_{geo} is given by the standard geometric optics model as (see Eq. 57 in Wentz and Meissner, 2000):

$$R_{geo} = R_0 - [r_0 + r_1 (\theta - 53) + r_2 (T_S - 288) + r_3 (\theta - 53)(T_S - 288)]W \tag{15}$$

The first term R_0 is the specular reflectivity given by Eq. 13 and the second term is the wind-induced component of the sea surface reflectivity. The r coefficients are given in Table 3 for all AMSR-2 channels used for calculating sea ice concentration.

The E_W term that accounts for both foam and diffraction effects is found to be a monotonic function of wind speed W as (see Eq. 60 in Wentz and Meissner, 2000):

$$E_W = m_1W \qquad\qquad W < W_1 \qquad\qquad (16a)$$

$$E_W = m_1W + 0.5(m_2 - m_1)(W - W_1)^2/(W_2 - W_1) \qquad W_1 \leq W \leq W_2 \qquad (16b)$$

$$E_W = m_2W - 0.5(m_2 - m_1)(W_2 + W_1) \qquad W > W_2 \qquad (16c)$$

where W_1 = 3 m/s and W_2 = 12 m/s for the v-pol, and W_1 = 7 m/s and W_2 = 12 m/s for the h-pol, respectively. The m coefficients are given in Table 3 for all AMSR-2 channels used for the sea ice concentration calculation.

Table 3. Model coefficients and constants for the sea surface with polarization

Freq. (GHz)	**19V**	**37V**	**37H**	**89V**	**89H**
r_0 (s/m)	−0.49E−3	−1.01E−3	1.91E−3	−1.53E−3	2.02E−3
r_1 (s/m-deg)	−0.53E−4	−1.05E−4	1.12E−4	−1.16E−4	1.30E−4
r_2 (s/m-K)	0.48E−5	1.27E−5	−0.36E−5	1.15E−5	0.00E−5
r_3 (s/m-deg-K)	0.31E−6	0.45E−6	−0.36E−6	−0.09E−6	−0.46E−6
m_1 (s/m)	0.00140	0.00257	0.00329	0.00260	0.00330
m_2 (s/m)	0.00736	0.00701	0.00660	0.00700	0.00660
E_{ice}	0.95	0.93	0.88	0.8	0.75
T_{mix}	0.75	0.95	0.70	0.97	0.97

V and H refer to vertical and horizontal, respectively.

Atmospheric radiation scattered by the sea surface $T_{B\Omega}$ can be approximated as (see Eq. 61 in Wentz and Meissner, 2000):

$$T_{B\Omega} = [(1 + \Omega)(1 - \tau)(T_D - T_C) + T_C]\, R, \qquad\qquad (17)$$

where R is the sea surface reflectivity given by Eq. 14, T_D is the down-welling brightness temperature given by Eq. 2 and T_C is a constant (2.7K) representing the cosmic background radiation temperature. Ω is the fit parameter given for v-pol and h-pol, respectively:

$$\Omega_v = [2.5 + 0.018(37 - v)](\sigma^2 - 70.0\sigma^6)\, \tau^{3.4} \qquad\qquad (18a)$$

$$\Omega_h = [6.2 - 0.001(37 - v)^2](\sigma^2 - 70.0\sigma^6)\, \tau^2 \qquad\qquad (18b)$$

where v is frequency (GHz) and σ^2 is the sea surface slope variance,

$$\sigma^2 = 5.22 \cdot 10^{-3}\, W \qquad\qquad v \geq 37 \text{ GHz} \qquad\qquad (18c)$$

$$\sigma^2 = 5.22 \cdot 10^{-3}[1 - 0.00748(37-v)^{1.3}]W \qquad v < 37 \text{ GHz} \qquad\qquad (18d)$$

The term $\sigma^2 - 70.0\sigma^6$ reaches a maximum at σ^2 = 0.069. For $\sigma^2 > 0.069$, the term is held at its maximum value of 0.046. Ω_h has a quadratic dependence on frequency with a maximum value at v = 37 GHz. For v > 37 GHz, both Ω_v and Ω_h are held constant at their maximum values. The approximation for Ω_v and Ω_h, given by Equations 18a and 18b are valid for the range of incidence angles from 52° to 56°.

The sea surface emissivity E is given by Kirchhoff's law to be

$$E = 1 - R. \tag{19}$$

Finally, the simplified radiative transfer equation for the brightness temperature from the atmosphere over open water (i.e. Eq. 1) and sea ice covered surfaces:

$$T_b = T_{BU} + \tau[(1 - C_{ice})E \cdot T_s + (1 - C_{ice})(1 - E)(T_{B\Omega} + \tau T_C)$$

$$+ C_{ice}E_{ice}T_{ice} + C_{ice}(1 - E_{ice})(T_{BD} + \tau T_C)] \tag{20}$$

where E_{ice} is the ice emissivity and the ice effective temperature T_{ice} has a linear relationship between sea surface and freezing point of 272 K.

$$T_{ice} = T_{mix} \cdot T_s + 272(1 - T_{mix}) \tag{21}$$

if $T_{ice} \leq 0$, then $T_{ice} = 0$; if $T_{ice} \geq 272$ K, then $T_{ice} = 272$ K. Both E_{ice} and T_{mix} are channel dependent, given in Table 3 for all AMSR-2 channels used for the ice concentration calculation. C_{ice} is the sea ice concentration, a fraction from 0 to 1 (indicating from no ice to 100% coved by ice).

4.2   Dynamical tie-points

The tie-points for ice and open water are the set of brightness temperatue values that correspond to ice concentrations of 100% and 0%, respectively. They are used in the ice concentration algorithms as a reference. The tie-points are derived by selecting T_b's from regions of known 100% open water and 100% ice. Usually these tie-points are static in time and space, but they can be adjusted to follow the seasonally changing signatures of ice and open water. Static tie-points are prone to be affected by sensor drift, inter sensor calibration differences and climatic trends in surface and atmospheric emission. The data must therefore be carefully calibrated before computing the ice concentrations. Here we use dynamic tie-points, a method that minimizes these unwanted effects, with or without prior calibration.

During winter, in the consolidated pack ice well within the ice edge, the ice concentration is very near 100 % (Andersen et al., 2007). This has been established using high resolution SAR data, ship observations and by comparing the estimates from different ice concentration algorithms. The apparent fluctuations in the derived ice concentration in the near 100% ice regime are primarily attributed to snow/ice surface emissivity variability around the tie-point signature and only secondarily to actual ice concentration fluctuations. In the marginal ice zone the atmospheric emission may be significant. The fluctuations due to atmospheric and surface emission are systematic. In fact, different algorithms with different sensitivity to atmospheric and surface emission compute very different trends in sea ice area on seasonal and decadal time scales (Andersen et al., 2007). This means that not only the sea ice area have a climatic trend, but the atmospheric and surface constituents affecting the microwave emission are also changing. For example, different wind patterns, water vapor and liquid water concentrations in the atmosphere, snow depth, fraction of perennial ice etc. In an attempt to compensate for the influence of these unwanted trends the tie-points are derived dynamically using a mean of the last 30 days of swath data. It is assumed that ice concentrations from the NT algorithm above 95 % are in fact near 100 % ice, and that the mean value of these data points can be used to derive the ice tie-point. The NT ice concentration is the initial guess before the iteration and the OSI SAF ice concentration does not depend on the NT ice concentration. The analysis of SAR data in Andersen et al. (2007) from the central arctic showed that during winter there is more than 99% ice cover. During strong ice drift divergence and during the summer there may be situations where this is not the case. However, during one month of tie-point data collection we are sure to have captured the situations with near 100% ice cover. The standard deviation of the tie-point is included in the total ice concentration error estimate which is the justification for this assumption.

Regions of open water are selected near the ice edge using the monthly NSIDC maximum ice extent climatology plus additional 100 km. There is no attempt to compensate explicitly for sensor drift or inter-sensor calibration differences between the seven different sensors used in the analysis. The dynamical tie-point method is in principle compensating for these problems in a consistent manner.

Dynamical tie-point algorithm summary:

1. For each swath grid point the NT ice concentration (static tie-points, Comiso et al. 1997) is added.

2. The atmospheric correction is applied based on the NT ice concentration and the NWP data.

3. The dynamical tie-points are computed using the swath data for one day i.e. the number of data points for the ice and the water tie-points, the coordinates for the ice line and for the water point. Dynamical tiepoints are computed separately for the Bristol algorithm, the Bootstrap algorithm and the algorithm 89 GHz linear. The two sets for the first two algorithms are used by the OSI SAF hybrid algorithm, and the sets for the last two algorithms are used by the TUD hybrid algorithm (see the next section).

4. The daily tie-point coordinates are combined into a 30 day running mean tie-point which is used in the further processing.

4.3   The ice concentration algorithm

A total of 30 algorithms retrieving Arctic sea ice concentration from satellite passive microwave data are described and compared in detail in the SICCI ATBD (ESA SICCI project consortium, 2013).

The analysis of atmospheric sensitivity in Andersen et al. (2006B) showed that the Bootstrap frequency mode algorithm (Comiso, 1986) had the lowest sensitivity to atmospheric noise over open water. Furthermore, the comparison to high resolution SAR imagery in Andersen et al. (2007) revealed that among the algorithms using the low frequency channels (19 and 37 GHz), the Bristol algorithm (Smith, 1996) had the lowest sensitivity to ice surface emissivity variability. In addition this algorithm had a low sensitivity to atmospheric emission in particular at high ice concentrations. Consequently, a hybrid algorithm has been established as a linear combination of two of the tested algorithms, the Bristol algorithm and the Bootstrap frequency mode algorithm. To ensure an optimum performance over both marginal and consolidated ice, and to retain the virtues of each algorithm, the Bristol algorithm is given little weight at low concentrations, while the opposite is the case over high ice concentrations.

The TUD ice concentration algorithm represents the Bootstrap algorithm (Comiso, 1986; Comiso et al., 1997) using high resolution and high frequency channels (Pedersen, 1998). The algorithm uses the Bootstrap algorithm in frequency mode to determine coarse resolution ice concentration almost independent of weather conditions. If the coarse resolution algorithm gives above zero ice concentration, the algorithm 89 GHz linear with dynamic tie-points is used to split the pixel with ice in four sub-cells according to a linear conversion of the polarization difference to ice concentration, whereas if the coarse resolution algorithm gives zero (or less) ice concentration, this value and the coarse resolution is maintained (ESA SICCI project consortium, 2013).

4.3.1 The OSI SAF hybrid algorithm

The Bootstrap algorithm (Comiso, 1986) is based on the observation of linear clustering of ice T_b's in scatter plots of T_{37V} vs T_{19V} whereas open water T_b's cluster around a single point. It assumes only two surface types: ice and open water, taking into account the variability of both to optimize the detection of small sea ice concentrations. The linear relationship yields the following simple formulation for the total ice concentration, $C_{bootstrap}$:

$$C_{bootstrap} = (T_b - T_b^W)/(T_b^I + T_b^W)*100, \tag{22}$$

where T_b is the measured brightness temperature, T_b^W and T_b^I are the open water tie-point and the ice tie-point, respectively, both in the unit of temperature.

The Bristol algorithm (Smith, 1996) is conceptually similar to the Bootstrap algorithm. In a three-dimensional scatter plot spanned by T_{19V}, T_{37V} and T_{37H} the ice T_b's tend to lie in a plane. The only difference to the Bootstrap algorithm is that instead of viewing the data in the T_{19V}, T_{37V} space, the Bristol algorithm views the data perpendicular to the plane in which the data lies, i.e. in a transformed coordinate system:

$$Bristol_x = T_{37V}+1.045T_{37H}+0.525T_{19H}, \tag{23a}$$

$$Bristol_y = 0.9164T_{19V}-T_{37V}+0.4965T_{37H}. \tag{23b}$$

The remaining analysis is identical to the Bootstrap algorithm.

The Bootstrap algorithm is used over open water and the Bristol algorithm is used over ice. At intermediate concentrations up to 40% the ice concentration is an average weighted linearly between the two algorithms, as shown in Eq. 24. This hybrid algorithm is the OSI SAF sea ice concentration algorithm.

$$C_{tot} = (1\text{-}weight)\, C_{bristol} + weight \cdot C_{bootstrap}, \tag{24a}$$

$$weight = (|threshold - C_{bootstrap}| + threshold - C_{bootstrap})/(2\; threshold), \tag{24b}$$

where *threshold* is 40%.

4.3.2 The TUD hybrid algorithm

The TUD hybrid algorithm is a combination of the coarse resolution ice concentration C_f determined by the Bootstrap algorithm in frequency mode and the high resolution ice concentration C_{89} determined by the algorithm 89 GHz linear with dynamic tie-points. Both are calculated by the Bootstrap algorithm (Eq. 22), with different input of brightness temperature, T_{19V} and T_{37V} for C_f and T_{89V} and T_{89H} for C_{89}.

A comparison between C_f and C_{89} shows that there are larger scatter, in particular at the low ice concentrations derived from 89 GHz than the lower frequency channels (Pedersen, 1998). In order to reduce the noise in C_{89}, the TUD algorithm is adjusted as:

If $C_{89} > 0$ and $C_f > 10$, the total ice concentration, C

$$C = sqrt(C_f \cdot C_{89}) \tag{25}$$

Otherwise, the total ice concentration, C

$$C = C_f. \tag{26}$$

4.4 Sea ice concentration uncertainties

Uncertainty estimates are needed when the ice concentration data are compared to other data sets or when the ice concentrations are assimilated into numerical models. The mean accuracy of some of the more common algorithms, used to compute ice concentration from SSM/I data, such as the NT and Bootstrap algorithms are reported to be 1-6 % in winter (Andersen et al., 2006A). This is also achieved with the OSISAF algorithm (Ivanova et al., 2015).

The polar atmosphere is generally transparent for microwave radiation in between the sounding channels called the atmospheric windows near 19, 37, 91, and 150 GHz. For typical polar atmospheric states the down-welling emission at the surface is about 5-15 K at 18 GHz, 20-40 K at 36 GHz, 30-100 K at 90 GHz. For comparison, the sea ice surface emission is typically 150-260 K. When computing the ice concentration using the atmospheric window channels, the atmospheric emission and scattering is an error source. The tie-points are typical ice and water signatures representative on a hemispheric scale. Deviations from the typical surface emission signatures result in ice concentration uncertainties. The AMSR-2 instrument has relatively large foot-prints on the ground, and the algorithms with the lowest sensitivity to both atmospheric and surface emissivity variability use T_b's at different frequencies with different foot-print size. Representing these large foot-prints on a finer, predefined grid results in a representativeness error. In addition there is the geo-location error, sensor noise, drift, and sea ice variability over the sampling period.

We assume the total uncertainty as

$$\sigma_{tot}{}^2 = \sigma_{algo}{}^2 + \sigma_{smear}{}^2, \tag{27}$$

where σ_{algo} is the inherent uncertainty of the concentration algorithm and σ_{smear} is the uncertainty due to resampling to a grid where the sensor footprint covers more than one pixel.

4.4.1   Algorithm and tie-point uncertainties

Both the water surface and ice surface emissivity variabilities result in ice concentration uncertainties. Emission and scattering in the atmosphere also affects the T_b's and the computed ice concentrations. Different algorithms have different sensitivities to these surface and atmospheric parameters (Andersen et al., 2006B). Further, both the atmospheric and surface parameters affecting the ice concentration estimates have climatic trends (Andersen et al., 2007). To minimize the uncertainties due to these two parameters, the T_b's are corrected using NWP data for atmospheric humidity and open water roughness in this reanalysis. The dynamical tie-points minimizes uncertainty due to the climatic trends in the atmosphere and on the ice surface on a hemispheric scale while regional trends may still exist.

The errors are computed using the hemispheric standard deviation of the measurements over open water and over near 100% ice respectively. The ice concentration algorithm provides ice concentrations which are greater than 100% and less than 0%. These unphysical concentrations are truncated in the processing. Therefore we write the ice concentration, *ic*:

$$ic = (1 - \alpha(ic))\, water + \alpha(ic)ice \tag{28}$$

where *ic* is the ice concentration calculated by the algorithm and *α* is the truncated ice concentration as a function of *ic*:

$$\alpha(ic) = \prod(ic)ic + H(ic - 1) \tag{29}$$

where $\prod(x)$ is the Boxcar function and *H*(x) the Heaviside step function. The functional dependency between *α* and *ic* is described by:

$$
\begin{array}{lll}
\alpha = 0 & & ic \le 0 \\[4pt]
\alpha = ic & & 0 < ic < 1 \qquad (30) \\[4pt]
\alpha = 1 & & ic \ge 1
\end{array}
$$

Using equation 28 and assuming the uncertainty for the ice and water part is independent, leads to a total algorithm uncertainty as

$$\sigma_{algo}(\alpha(ic)) = \sqrt{(1 - \alpha(ic))^2\, \sigma_{water}^2 + \alpha^2(ic)\sigma_{ice}^2} \quad , \tag{31}$$

where

$$\sigma_{water} = \sigma(IC(P_{openwater})) \tag{32}$$

and open water is determined by a monthly varying ocean mask, *IC* is the functional mapping of the ice concentration algorithm and *Pc* denotes the set of swath pixels for all swaths (used for calculating the daily product) selected on the condition *C*. The condition *C* is either ice or water.

The standard deviation of the ice concentrations is given by

$$\sigma_{ice} = \sigma(IC(P_{ocean,NT>0.95})) \quad , \tag{33}$$

where the NT algorithm finds ice concentrations greater than 0.95.

4.4.2   Representativeness error

Foot-print sizes for the channels used for ice concentration mapping range from about 18 km for the 19 GHz channels to about 10 km for the 37 GHz channels. Foot-prints of uneven size are combined in the algorithms when computing the ice concentration. The foot-print ice concentration is represented on a predefined grid. The ice concentration data are represented on a finer grid (e.g. 10 or 12.5 km) than the sensor resolution. This is known as smearing. The combination of foot-prints of uneven size in the ice concentration algorithm results in an additional smearing effect. This we call the foot-print mismatch error. The smearing and the foot-print mismatch error cannot be estimated separately. However, the combined error can be estimated if all other error sources and the ice cover reference are known *a priori*. It can also be simulated using high resolution ice concentration reference data and a model for the satellite measurement foot-print patterns. For a grid resolution of 10 km, the AMSR-2 TUD ice concentration has smearing uncertainty component of 11% and for the 12.5 km grid it is 10%. More details in simulating the smearing uncertainties for different algorithms and ice concentrations are available in [RD.2] and [RD.3].

4.4.3   Geo-location error

Geolocation error occur due to uncertainties in the orientation of the satellite. For AMSR2, the RMSE geolocation error is approximately 5 km for the 6.9 GHz channel (~10% of the beam FWHM footprint dimensions), reducing to 1 km for the 89 GHz channel (~20% of the beam FWHM footprint dimensions).

5. Level 3 processing

In level 3 processing, the sea ice concentration calculated from the satellite swath (i.e. not gridded) data for one day are concatenated into one daily map of ice concentration on OSISAF grids. Coastal correction and masking fields are also applied to the daily ice concentration maps.

5.1 Daily gridding and uncertainty estimates

The computed ice concentration estimates in swath projection for one day are concatenated and gridded onto the OSISAF grid as daily level 3 products. The OSI SAF grid is a polar stereographic 10 km grid defined for the northern and southern hemisphere. Several AMSR-2 ice concentration estimates from the separate swaths are combined in each grid point of the OSI SAF grid. The radius of influence is the radius around each grid pixel in meters to search for neighbors in the swath. It depends on: 1) the variance of the ice concentration estimate, and 2) the distance between the center of the AMSR-2 node and the predefined grid-point. The variance of the AMSR-2 ice concentration estimates is scaled with the ice concentration and variability within the grid cell.

The daily gridding searches for all satellite observation within 24 hours, centered on 12:00 UTC, and grids these to the final output grid. The *pyresample* python library and the function of *resample_gauss* is applied. The observations within one grid cell are averaged, using a Gaussian weighting:

$$weight = exp(-dist^2 / \sigma^2), \tag{34}$$

where

$$\sigma = FWHM/(2sqrt(2ln2)) \tag{35}$$

dist is the distance between the observation and center of grid point, and *FWHM* is 3 dB level of beam footprint. For low resolution channels (19 and 37 GHz) 18 km is used (see Table 1) and σ is approximately 7.64 km. A radius of influence of two times *FWHM* is used here and the gauss resampling is calculated from 3 dB FOV levels.

A similar gridding/averaging is applied for the uncertainty estimates. The uncertainty is calculated based on all the swath pixels contributing to a level 3 ice concentration product. As described in the pyresample documentation (https://pyresample.readthedocs.org), uncertainty estimates in the form of weighted standard deviation are obtained also from the Gaussian weighting function (Eq. 33). The principle, used to calculate the uncertainty, is to consider the resampled values as a weighted average of values sampled from a statistical variable. An estimate of the standard deviation of the distribution is calculated using the unbiased weighted estimator given as:

$$std = \sqrt{(V_1/(V_1^2 + V_2)) \sum_i w_i(x_i - r)^2}, \tag{36}$$

where r is the result of the resampling, x_i is the value of a contributing neighbour and w_i is the corresponding weight. The coefficients are given as $V_1 = \sum_i w_i$ and $V_2 = \sum_i w_i^2$. The standard deviation is only calculated for elements in the result where more than one neighbour has contributed to the weighting.

5.2 Land spillover correction

Observations in the coastal zone are a mixture between land and water/sea ice. Land has similar signatures to sea ice, and the algorithms therefore overestimate the sea ice concentration in these areas. This problem is known as land spill-over. A land mask is applied to ice concentration maps; however, due to *land spillover,* erroneous ice concentrations are still observed along the coast. A land spillover correction scheme is applied in order to mitigate the problem. The objective of the scheme is to eliminate erroneous and keep valid

ice concentration data. The following procedure, modified from the one given in Markus et al. (2009), is applied:

1. The pixels of the polar-sterographic grid are classified with respect to their distance in pixels from the coast. Beside the coast they are labeled *1*, the pixels next furthest out are label *2* and the next furthest out again are labeled *3*. Pixels further away than three pixels are labeled 0.

2. Pixels with classes 1 or 2 are assessed for erroneous sea ice concentrations by analysing the 11 by 11 pixel neighbourhood (equivalent to 110 km). This area encompasses the AMSR-2 antenna pattern. Pixels with values of 3 or 0 will not be changed.

3. In the 11 by 11 pixel neighborhood, if the coastal mask is 1 or 2 and ice concentration is below the theoretical value of land spillover the ice concentration is set to 0.

4. In the 11 by 11 pixel neighborhood, if the coastal mask is 1 or 2 and all type 3 pixels have ice concentration less than 15%, the signal is assumed to be due to noise, and the ice concentration is set to 0.

5. The theoretical concentration caused by land spillover is determined as follows: Calculate an average sea ice concentration for the 11 by 11 pixel box, assuming all the ocean pixels have zero ice concentration and all the land pixels have a concentration of 90%, approximating a theoretical concentration caused by land spillover only.

If the ice concentration is less than or equal to this value, the pixel at centre of box is set to 0.

6. References

Andersen, S., L. Toudal Pedersen, G. Heygster, R. Tonboe, and L Kaleschke, Intercomparison of passive microwave sea ice concentration retrievals over the high concentration Arctic sea ice. *Journal of Geophysical Research* 112, C08004, doi10.1029/2006JC003543, 2007.

Andersen, S., R. T. Tonboe and L. Kaleschke. Satellite thermal microwave sea ice concentration algorithm comparison. *Arctic Sea Ice Thickness: Past, Present and Future*, edited by Wadhams and Amanatidis. Climate Change and Natural Hazards Series 10, EUR 22416, 2006A.

Andersen, S., R. Tonboe, S. Kern, and H. Schyberg. Improved retrieval of sea ice total concentration from spaceborne passive microwave observations using Numerical Weather Prediction model fields: An intercomparison of nine algorithms. *Remote Sensing of Environment104, 374-392*, 2006B.

Comiso J.C, D.J. Cavalieri, C.L. Parkinson, and P. Gloersen. Passive microwave algorithms for sea ice concentration: A comparison of two techniques. *Remote Sensing of Environment* 60, 357-384, 1997.

Comiso J.C. Characteristics of arctic winter sea ice from satellite multispectral microwave observations. *Journal of Geophysical Research* 91(C1), 975-994, 1986.

ESA SICCI project consortium. D2.6: Algorithm Theoretical Basis Document (ATBDv1), ESA Sea Ice Climate Initiative Phase 1 Report SICCI-ATBDv1-04-13, version 1.1, 2013.

Imaoka, K., M. Kachi, M. Kasahara, N. Ito, K. Nakagawa and T. Oki. Instrument performance and calibration of AMSR-E and AMSR2. International Archives of the Photogrammetry, Remote Sensing and Spatial Information Science, 38(8), 13-18, 2010.

Ivanova, N., L. T. Pedersen, R. T. Tonboe, S. Kern, G. Heygster, T. Lavergne, A. Sørensen, R. Saldo,G. Dybkjær, L. Brucker, and M. Shokr. Inter-comparison and evaluation of sea ice algorithms: towards further identification of challenges and optimal approach using passive microwave observations. The Cryosphere, 9, 1797–1817, 2015.

Markus T, Cavalieri D. The AMSR-E NT2 Sea Ice Concentration Algorithm: its Basis and Implementation. *Journal of The Remote Sensing Society of Japan*. 2009; 29 (1):216-225.

Pedersen, L.T. Chapter 6.2 in Sandven et al. IMSI report no. 8. Development of new satellite ice data products (Chapter 6.2). Bergen, Norway: NERSC Technical Report no.145, Nansen Environmental and Remote Sensing Center, Bergen, Norway, 1998.

Smith, D. M. Extraction of winter total sea ice concentration in the Greenland and Barents Seas from SSM/I data. *International Journal of Remote Sensing* 17(13), 2625-2646, 1996.

Wentz, F. J. A well-calibrated ocean algorithm for SSM/I. *Journal of Geophysical Research* 102(C4), 8703-8718, 1997.

Wentz, F. J., Meissner, T. (2000). AMSR ocean algorithm version 2. RSS Tech. Proposal 121599A-1, Remote Sensing Systems, Santa Rosa, California.